Nano Science and Nano Technology

An Indian Journal

Trade Science Inc.

Full Paper

Synthesis of silver incorporated ZnO nanostructures by different methods and investigation of their photocatalytic and antibacterial efficiency

B.Divband*, M.Khatamian
Inorganic Chemistry Department, Faculty of Chemistry, University of Tabriz, C.P. 51664, Tabriz, (IRAN)
E-mail : baharakdivband@yahoo.com

ABSTRACT

In this paper, Ag/ZnO photocatalysts with different Ag loadings were prepared by photo reduction, chemical reduction and polyacrylamide-gel methods. The Ag/ZnO photocatalysts were characterized by XRD, SEM, TEM, EDX and DRUV-vis methods. The results of the photocatalytic degradation of 4-NP in aqueous suspensions showed that silver ions doping greatly improved the photocatalytic efficiency of ZnO nanocrystallites. The enhancement of photocatalytic activity is due to the fact that the modification of ZnO with an appropriate amount of Ag can increase the separation efficiency of photogenerated electrons and holes in ZnO, and the improvement of photo stability of ZnO is attributed to a considerable decrease of the surface defect sites of ZnO after the Ag loading. The chemisorptions of molecular oxygen and the chemisorption of atomic oxygen on Ag in the Ag/ZnO photocatalysts were observed. It was found that the metallic Ag in the Ag/ZnO photocatalysts does play a new role of O_2 chemisorption sites except for electron acceptor, by which chemisorbed molecular oxygen reacts with photogenerated electrons to form active oxygen species, and thus facilitates the trapping of photogenerated electrons and further improves the photocatalytic activity of the Ag/ZnO photocatalysts. Also the method of preparation is regarded as important factors for determining photocatalysis. The best photocatalytic performance was exhibited for Ag/ZnO prepared by polyacrylamide gel method in comparison with chemical reduction and photo reduction method and the optimum Ag content was approximately 0.5%. With the appearance of microbial organisms resistant to multiple antibiotics, also, increase nosocomial infection, antibacterial effects of nanocomposites have attended by the many researchers in recent years. In the present work, the antibacterial properties of Silver incorporated zinc oxide nanoparticles were investigated using Escherichia coli.   © 2013 Trade Science Inc. - INDIA

INTRODUCTION

In the past decades, the scientific and engineering interest in the application of semiconductor photocatalysis has grown exponentially[1–8]. ZnO can act as a sensitizer for light-induced redox due to its electronic

Full Paper

structure, which is characterized by a filled valence band and an empty conduction band. When a photon with an energy of hv matches or the bandgap energy, E_g, of the semiconductor, an electron, e_{cb}^-, from the valence band (VB), is excited and enters into the conduction band, CB, leaving a hole, h_{vb}^+ behind. Excited state conduction band electrons and valence band holes can recombine and release energy as heat, get trapped in metastable surface states, or react with electron donors and electron acceptors adsorbed on the semiconductor surface or within the surrounding electrical double layer of the charged particles. If a suitable scavenger or surface defect is available to trap the electron or hole, recombination is prevented and subsequent redox reactions may occur. Usually, undoped ZnO exhibits n-type conductivity, which can be ascribed to the asymmetric doping limitations[9] and propensity to defects or impurities[10,11]. P-type doping of ZnO films has been achieved using P,[12] N,[13] As,[14] Li,[15] Sb,[16-19] and Ag[20,21] as dopants. These dopants and defect complexes, introduced through synthesis techniques, can define the type of conductivity[22] and optical[23,24] and electrical properties[24,25] of ZnO. It has been found that the photocatalytic performance of ZnO can be greatly improved by constructing a silver–ZnO composite because of the increase in the rate of electron-transfer process by metal silver[2–4]. Pure Ag- or Sb-doped ZnO has been effectively prepared by pulsed laser deposition[17,20,26] radio frequency magnetron sputtering,[27,28] and molecular beam epitaxy[29]. For preparation of doped ZnO nanoparticles several methods, such as microwave heating process[30], co-precipitation[31], chemical vapor synthesis[32] and others were used. Although the aforementioned methods can be employed to produce doped ZnO nanoparticles, they have some drawbacks, such as requirement of a large quantity of solution and organic materials, long processing time, and unsuitable for large scale production or ill crystallinity and wide particle size distribution. Thus, it is of practical importance to seek for a novel method that does not have those drawbacks for preparation of doped ZnO nanoparticles as photocatalysts materials.

Very recently, the polymer pyrolysis method has been developed for preparation of ferrite nanoparticles such as $MnFe_2O_4$, $NiFe_2O_4$, and $ZnFe_2O_4$[33], ZnO supported on zeolites and Ln doped ZnO[34,35]. This method is easily operated and versatile for various metals and thus should also be suitable for preparation of metallic ion doped n-type semiconductors. In the present work, the polyacrylamide-gel method, photo reduction and chemical reduction methods were used to synthesize Ag- modified ZnO nanoparticles. At last their photocatalytic activities are compared for degradation of 4-nitro phenol.

Also with the appearance of microbial organisms resistant to multiple antibiotics, also, increase nosocomial infection, antibacterial effects of nanocomposites have attended by the many researchers in recent years. In the present work, the antibacterial properties of Silver incorporated zinc oxide nanoparticles were investigated using Escherichia coli.

EXPERIMENTAL

Materials

Zinc acetate dihydrate, nitric acid, citric acid, acryl amide, 2, 2′-azoisobutyronitrile (AIBN), $AgNO_3$ were obtained from Merck.

Measurements

Differential thermal analysis and thermal gravimetric (DTA-TG) was conducted at a heating rate of 5°C min^{-1}. X-ray diffraction patterns (XRD) were collected using a Siemens D500 diffractometer with Cu kα radiation (λ=1.5418 A° and θ=4-80°) at room temperature. Scanning electron microscope (Philips XL30) equipped with energy dispersive X-ray (EDX) facility was used to capture SEM images and to perform elemental analysis. The SEM sample was gold coated prior to examination and SEM was operated at 5kV while EDX analysis was performed at 15 kV. UV-Vis diffuse reflectance spectra (UV-Vis DRS) were recorded in air at room temperature in wavelength range of 200-800 nm using a Scinco 4100 spectrophotometer. The band gap energy was calculated by the following equation:

λg= 1240/Eg,

Where λg is the wavelength of the characteristic absorption peak value; Eg is the band gap energy.

The products have been characterized by transmission electron microscope (TEM) and energy-dispersive X-ray analysis (EDX). TEM studies, combined

with EDX were carried out on a Zeiss LEO 912 Omega instrument, operating at 120 kV. TEM specimens were made by evaporating one drop of solution of sample in ethanol onto carboncoated copper grids. Grids were blotted dry on filter paper and investigated without further treatment. The Brunauer-Emett-Teller (BET) surface area of the catalysts was measured by N2 adsorption–desorption isotherm at liquid nitrogen temperature using NOVA2000 (Quantachrome, USA).

Preparation of materials

(a) Polyacrylamide-gel method (A_nZ1)

In a typical experiment, 0.17g (0.774 mmol) $Zn(CH_3CHOO)_2.2H_2O$ was dissolved in 2ml dilute nitric acid (2 mol L^{-1}) and 0.3g citric acid (1.6mmol) was added in order to accelerate dissolution of $Zn(CH_3CHOO)_2.2H_2O$. The mixture were kept stirring for 2h. The final PH was controlled as 6-7 by using dilute ammonia. Subsequently, the monomers of acrylamide (0.3g) were added and the resulting solution was stirred for 1h, then the aqueous solution of $AgNO_3$ was dropped into the transparent solution under stirring for 15 minutes, at last heated in a water bath and during the whole process, the system was continuously stirred. The solution became gradually transparent with temperature rising. When the temperature reached about 80 °C, a small amount of compound initiator AIBN ($C_8H_{12}N_4$) was added into the solution and polymerization occurred quickly and transparent polymeric resin was obtained without any precipitation. At last, the gel was dried at 100 °C for 24 h to yield a xerogel. The xerogel was heated in a laboratory furnace at 300 °C for 10h to burn out the organic residues and calcined at higher temperature (550°C) for 5h. The molar ratio of Ag:Zn was 0:100, 0.1:100, 0.5:100, 1:100 & 2:100. The final products were obtained, which were designed as A_nZ1 (n= 0, 0.1, 0.5, 1 & 2) respectively.

(b) Photo reduction method (A_nZ2)

4.288g (0.02 mol) $Zn(CH_3CHOO)_2.2H_2O$ was dissolved in 15ml of ethanol (96%) at room temperature in an ultrasonic bath for 1h. Then the clear solution was heated under reflux and stirring for 3h and during reflux 40ml of distilled water was added drop wise, the mixture solution became milky. Next, the aqueous solution of $AgNO_3$ was dropped into the milky solution under vigorous stirring for 20 minutes. The reaction

mixture was stirred for 2h under UV-C (30w) lamp to reduce adsorbed Ag^+ to Ag particles. The precipitate was separated from solution by centrifugation at 1500 rpm for 5 min and washed with deionized water repeatedly to remove the residual Ag^+ and then dried at 70°C for 10h and finally calcined at 550°C for 4h. The molar ratio of Ag:Zn was 0.1:100, 0.5:100, 1:100 & 2:100. The final products were obtained, which were designed as A_nZ2 (n= 0, 0.1, 0.5, 1 & 2) respectively.

(c) Chemical reduction method (A_nZ3)

4.288g (0.02 mol) $Zn(CH_3CHOO)_2.2H_2O$ was dissolved in 20ml of distilled water at room temperature in an ultrasonic bath for 1h. Then the clear solution was heated under reflux and stirring for 3h, the mixture solution became milky. Next, the aqueous solution of $AgNO_3$ was dropped into the milky solution under vigorous stirring for 20 minutes. Appropriate amount of NaBH4 solution was added to the milky solution to reduce adsorbed Ag^+ to Ag particles. The molar ratio of Ag:Zn was 0.1:100, 0.5:100, 1:100 & 2:100. The final products were obtained, which were designed as A_nZ3 (n= 0, 0.1, 0.5, 1 & 2) respectively.

Catalytic activity

Degradation of 4-nitrophenol (4-NP) was chosen as the reaction to quantify the photocatalytic reactivity of each sample. The experiments were carried out with 50 ml 4-NP (10ppm) solution prepared with distilled water in 150 ml beakers. Prior to illumination, the reaction suspension was first magnetically stirred in the dark for 15 minute to ensure the establishment of adsorption/desorption equilibrium of the concerned chemical substances on the surface of the catalysts. Then the beakers were put under the ultraviolet light in the appropriate stirring. Proper amount (0.1g) of catalysts was added to the solution. Samples were taken out at given time intervals and the solution was centrifuged at 1500 rpm for 5 min and then filtered to remove the catalyst particles completely. The analysis of concentration of 4-NP in filtered solution was performed by means of a Shimadzu UV-240 spectrophotometer. The absorption band around 315 nm (for the 4-NP) decreased as a function of time for each catalyst. This can be attributed as oxidative degradation of the 4-NP by the catalysts. Direct band gap excitation of the semiconductor results in electron-hole separation. Photo generated holes oxi-

Full Paper

dize the 4-NP at the catalysts' surface.

The decrease in the absorbance seen at 315 nm for the 4-NP as a function of time can be used to estimate the percentage degradation of the 4-NP. The extent of equilibrium adsorption was determined from the decrease in 4-NP concentration. From the adsorption experiments, the percentage of 4-NP adsorbed on the catalyst surface was determined from the following equation:

$$\text{adsorption}(\%) = \frac{C_o - C_t}{C_o} \qquad (1)$$

where C_0 is the initial concentration of 4-NP and C_t is the concentration of 4-NP at time 't' (min).

Antimicrobial activities

The agar plate method was taken to evaluate the antimicrobial activities of Ag/ZnO prepared by different methods compared with the positive control and pure ZnO. Escherichia coli 745 (E. coli) was used as the test bacteria. The bacterial culture was diluted by sterile distilled water to 10^8 CFU/ml (CFU: Colony Forming Unit). A loop of the suspension was inoculated on nutrient plates with the sample spread. Then the plates with bacteria were incubated at 37°C for 48 h. A corresponding plate without any nanoparticles was used as a positive control. Finally, the antimicrobial activities of the samples were evaluated by the diameter of the test microorganism. All the experiments were repeated four times. The results were averaged.

RESULT AND DISCUSSION

Proposed mechanisms for various preparation methods of Ag/ZnO nanoparticles

The co-polymeric precursor compound (A_nZ1) is schematically represented in Figure 1. As shown, the Zn (II) and Ag (I) ions are bound by the strong ionic bonds between the polymeric chains. This uniform immobilization of metallic ions in the polymer chains favors the formation of uniformly Ag-modified ZnO nanoparticles in the following pyrolysis process. Also comparison to the other used methods this procedure lead to the finest particle size as shown in Figure 4. Furthermore, this method is simple to operate and very suitable for industrial production of nanoparticles. In addition, this method can be versatile to facilely synthe-

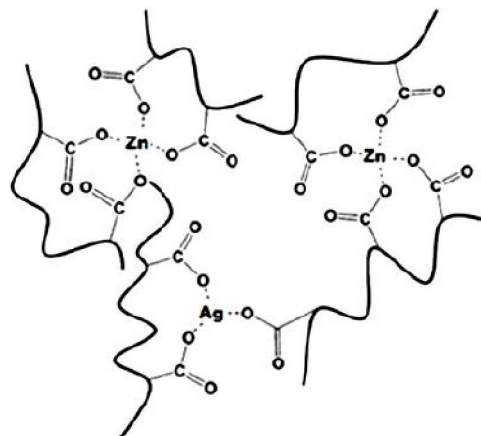size other metallic ion doped n-type semiconductor, such as In, Ga, Al doped ZnO.

Figure 1 : Schematic representation of polymeric chain of the co-polymeric precursor of Zn-Ag polyacrylates.

To clarify the chemical reactions of the co-polymeric precursors occurring in the pyrolysis process, TG and DSC curves of the copolymeric $A_{0.5}Z1$ precursors were measured and shown in Figure 2. In the TG curve of $A_{0.5}Z1$ precursor, there are two mass losing processes present at room temperature to about 160°C and 160–520°C. The first step of mass loss is corresponding to a small endothermal peak in the DSC curve, which is associated with the removal of the residual water, acetate and un-polymerized acrylic acid molecular in the precursor. The second step of mass decomposition of polymer precursor occurs at the temperature range of 160–520 °C and at the same time a high exothermic peak in the DSC curve is observed at around 400–530 °C, which is likely to be associated with the decomposition of Ag–Zn polyacrylate into $A_{0.5}Z1$ nanoparticles. It is noted that the mass is almost unchanged above the decomposition temperature of 520 °C, indicating that the final decomposed products are $A_{0.5}Z1$ nanoparticles. Hence, 550 °C was chosen as the calcination temperature in preparation of A_nZ1 nanoparticles.

The A_nZ2 photocatalysts were prepared by photoreduction of Ag^+ on ZnO with ethanol as hole scavenger. Upon UV irradiation, electrons in the valence band of ZnO are excited to its conduction band with simultaneous generation of the same amount of holes left behind. Therefore, we think that ZnO serves as electron source for the reduction of silver cations. It is known that ZnO easily adsorbs Ag^+ cations at its surface. Once

cationic silver clusters like Ag_2^+ are formed, the reduction process is facilitated[36]. The photo-generated holes in ZnO are captured by ethanol.
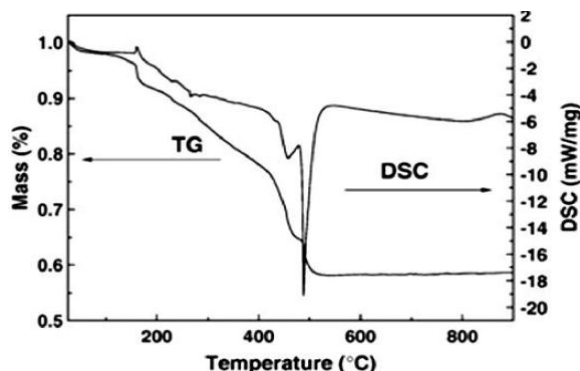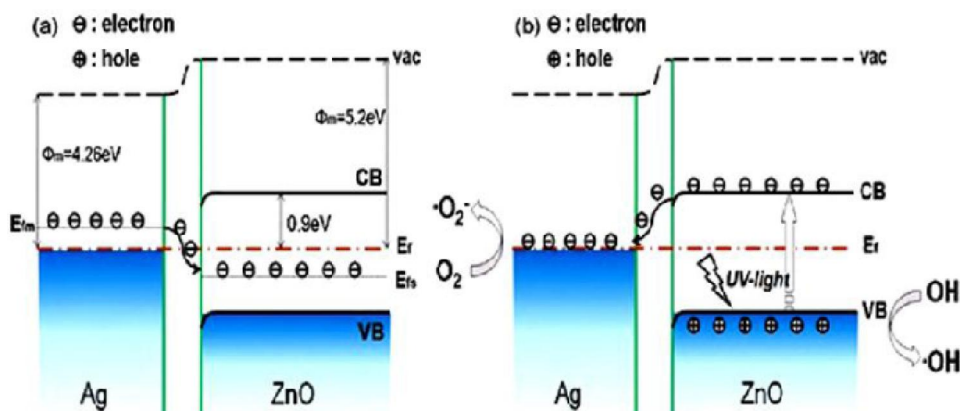

Figure 2 : TG-DSC curves of $A_{0.5}Z1$ precursor.

Scheme 1a shows the band structures and the Fermi energy levels of Ag and ZnO junction. Because the Fermi energy level of Ag (E_{fm}) is higher than that of ZnO (E_{fs}), part of electrons transferred from Ag to ZnO until the two systems attained equilibrium and a new Fermi energy level (E_f) was formed[37,38]. Scheme 1b shows the proposed charge separation process and the photocatalytic mechanism of as-prepared Ag/ZnO samples under UV irradiation. Due to that the energy level of CB for ZnO is higher than the Fermi energy level of Ag, the photoinduced electrons are transferred to the metallic Ag. Then the electrons in the Ag sinks can be trapped by the chemisorbed O_2 and the hole can be captured by the surface hydroxyl.

Scheme 1 : (a) The band structures of Ag and ZnO junction and the fermi energy level equilibrium without UV irradiation. (b) The proposed charge separation process and the photocatalytic mechanism of as-prepared Ag/ZnO samples under UV irradiation. The electrons in the Ag sinks can be trapped by the chemisorbed O_2 and the hole can be captured by the surface hydroxyl.

The A_nZ3 photocatalysts were prepared by chemical reduction of Ag^+ on ZnO in presence of $NaBH_4$. $NaBH_4$ is a metal hydride with strong reduction capacity and high hydrogen content. It releases its hydrogen as a result of hydrolysis. This is a rapid reaction at room temperature.

$$Ag^+ + e^- \rightarrow Ag, E^0 = 0.79V \qquad (2)$$

$$Zn^{2+} + 2e^- \rightarrow Zn, E^0 = -0.76V \qquad (3)$$

According to the E^0 of the Ag^+ and Zn^{2+}, silver ions were reduced by $NaBH_4$ and after calcined at 550°C, Ag/ZnO was prepared.

Structural and morphological characterization of Ag/ZnO nanoparticles

Figure 3 shows XRD patterns of Ag/ZnO nanoparticles recorded in the range of 20-70° with a scanning step of 0.02° by various preparation methods

and different Ag loadings. The observed diffraction peaks of the pure ZnO catalyst can be indexed to those of hexagonal wurtzite ZnO (PCPDF79-0207). No characteristic peaks of impurity phases such as Zn or $Zn(OH)_2$ were observed for all samples. As can be seen from Figure 3a, b and c, in all cases, after lower Ag loading ($\leq$0.5 wt%) on the ZnO, no characteristic diffraction peak corresponding to Ag or Ag compound impurity phase and no detectable structural change is observed for the ZnO catalyst, but with higher Ag loading ($\geq$1.0 wt%), It should be pointed out that a residual phase of silver is observed by XRD. According to some previous reports, Ag can be incorporated in ZnO system either as a substituent for zinc ions or as an interstitial atoms[39,40]. If the silver is substituted for Zn^{2+}, a corresponding peak shift would be expected in the XRD. In any of our modified samples, no such shift in the

peak position was observed. This indicates the segregation of Ag particles in the grain boundaries of ZnO crystallites rather than going into lattice of ZnO, or only an insignificant quantity may be going to the substitutional Zn site.
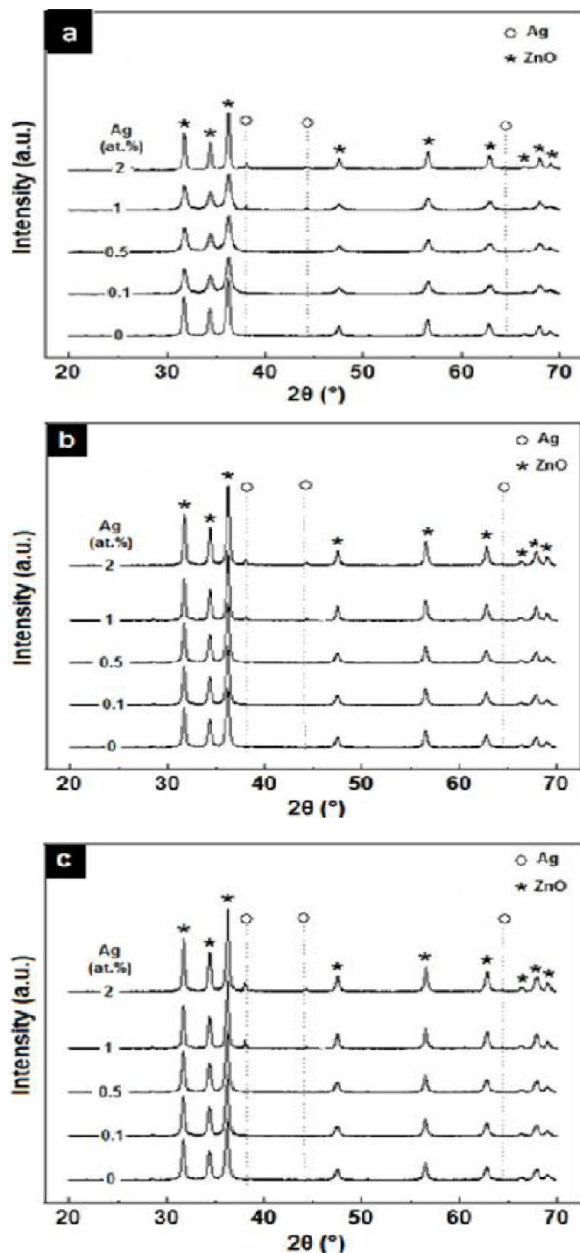

Figure 3 : XRD patterns of the Ag/ZnO photocatalysts with different Ag loadings:a)polyacrylamide-gel method(A_nZ1), b) Photo reduction method (A_nZ2), c) Chemical reduction method (A_nZ3).

The morphologies of the as-prepared products were investigated using TEM. Figure 4(a) - (c) shows the TEM images of $A_{0.5}Z1$, $A_{0.5}Z2$ and $A_{0.5}Z3$ respectively. The SEM image of as-synthesized A_nZ1 is also shown

in Figure 4(e). Interestingly It is clear that the sample is composed of lots of fluffy spheres with the diameter in the range of 1–2 μm. To know more about this strange structure, the middle part of the sphere is magnified and presented in the inset in 4(e). It is found that the ZnO sphere is constructed by lots of crossed nanosheets with average thickness of ~20nm and a large amount of "hollow lattice" present inside the sphere. Apparently, the synthesized A_nZ1 possesses a 3D hierarchical micro\nanostructure with a specific crossed arrangement of nanosheets.

Figure 4(b,c) indicates that Ag/ZnO nanocomposites are almost hexagonal (spherical) in shape. The mean particle size of them are 50-75 nm.
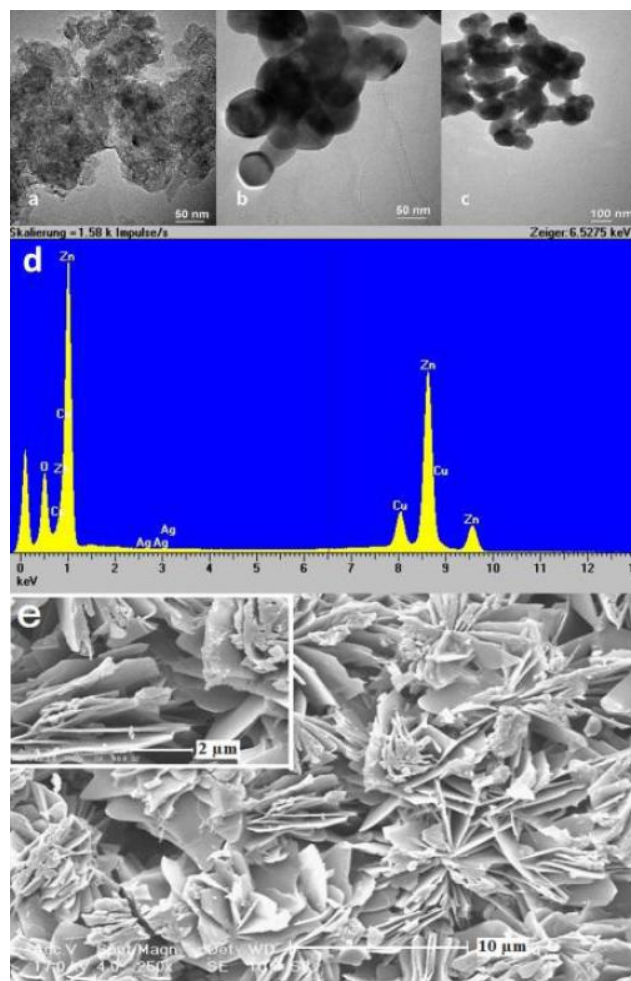

Figure 4 : TEM images of, a: $A_{0.5}Z1$, b: $A_{0.5}Z2$, c: $A_{0.5}Z3$ nanoparticles and d: EDX spectrum of $A_{0.5}Z1$, e: SEM image of $A_{0.5}Z1$.

Energy dispersive X-ray spectroscopy (EDX) analysis (Figure 4d), confirms that Ag/ZnO nanocomposite materials only consists silver, zinc and

oxygen. The presence of Cu and carbon signals arises from the TEM gird. Apart from that no other element peaks could be detected.

The diffuse reflectance spectra (DRS) of Ag–ZnO prepared by different methods are shown in Figure 5. The little change of the Eg of the samples also explains why the catalysts do not show high activity under the visible light. The top absorption peaks of ZnO, A_nZ1, A_nZ2, A_nZ3 occur at the wavelength of 365nm (3.39eV), 373nm (3.32eV), 372nm (3.33eV) and, 374nm (3.31eV), respectively.
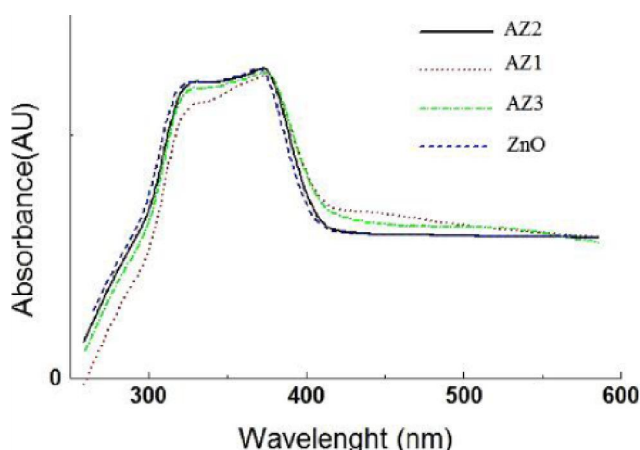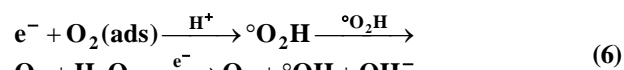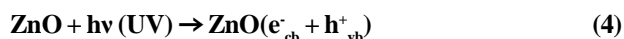

Figure 5 : DRS spectra of A_nZ1, A_nZ2, A_nZ3 and ZnO.

Catalytic activity

The results of the photocatalytic degradation of 4-NP in aqueous suspensions showed that silver modification greatly improved the photocatalytic efficiency of ZnO nanocrystallites. The enhancement of photocatalytic activity is due to the fact that the modification of ZnO with an appropriate amount of Ag can increase the separation efficiency of photogenerated electrons and holes in ZnO, and the improvement of photo stability of ZnO is attributed to a considerable decrease of the surface defect sites of ZnO after the Ag loading. The chemisorptions of molecular oxygen and the chemisorption of atomic oxygen on Ag in the Ag/ZnO photocatalysts were observed. It was found that the metallic Ag in the Ag/ZnO photocatalysts does play a new role of O_2 chemisorption sites except for electron acceptor, by which chemisorbed molecular oxygen reacts with photogenerated electrons to form active oxygen species, and thus facilitates the trapping of photogenerated electrons and further improves the photocatalytic activity of the Ag/ZnO photocatalysts. There-

fore, the higher the dispersity of Ag clusters and/or nanoparticles on the surface of ZnO is, the higher the photocatalytic activity of Ag/ZnO photocatalyst should be. This can be understood based on the proposed charged separation of Ag/ZnO under UV irradiation shown in scheme 1. Because the bottom energy level of the conduction band (CB) of ZnO is higher than the new equilibrium Fermi energy level (E_f) of Ag/ZnO, the photoexcited electrons on the CB under UV irradiations could transfer from ZnO to the Ag particles. It has been proposed that the charge separation is the outcome of a Schottky barrier formed at the metal–semiconductor interface[41,42]. The possible mechanistic pathway of Ag/ZnO for degradation of 4-NP can be proposed as follows:

$$ZnO + h\nu \ (UV) \rightarrow ZnO(e^-_{cb} + h^+_{vb}) \qquad (4)$$

$$Ag \rightarrow Ag^+ + e^- \qquad (5)$$

$$e^- + O_2(ads) \xrightarrow{H^+} {}^\circ O_2H \xrightarrow{{}^\circ O_2H}$$
$$O_2 + H_2O_2 \xrightarrow{e^-} O_2 + {}^\circ OH + OH^- \qquad (6)$$

$$Ag^+ + e^- \rightarrow Ag \qquad (7)$$

$$h^+_{vb} + OH^- \rightarrow {}^\circ OH \qquad (8)$$

$${}^\circ OH + 4\text{-}NP \rightarrow degradation \ products \qquad (9)$$

Also it is observed that with increasing the time up to 3h, the percentage of degradation of 4-NP increases. This is because of the fact that with increase in the irradiation time the number of photons absorbed increases, producing more amount of OH° by facilitating the oxidation of 4-NP.

At the end of the course of the phototcatalysis, the solution became colorless, odorless and transparent. From the absorption spectra, it can be seen that there is no peaks observed on the UVA region, probably because the ring of phenol was broken down into pieces and there is no alkene compounds formed. It is speculated that some alkanols might be the typical intermediates during the course of photocatalytic degradation. Since the 4-NP was extensively used as indicator for the photocatalytic reactions, detailed discussion for the intermediates and their toxicity were not discussed in this paper.

The photocatalytic activity of the catalyst depends upon the crystallinity, surface area and particle morphology[43] and these factors which depend on the method of preparation are regarded as important fac-

Full Paper

tors for determining photocatalysis. Figure 6 shows the effect of preparation methods on photocatalytic degradation of 4-NP.
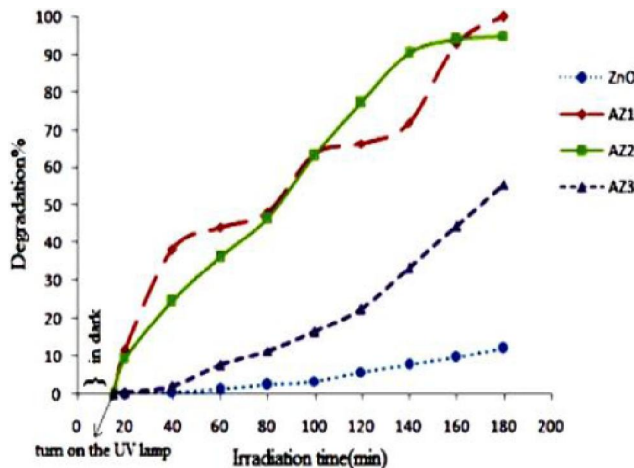

Figure 6 : Effect of preparation methods on the photocatalytic degradation of 4-NP.

From the Figure 6, it is observed that the best photocatalytic performance towards the oxidation of 4-NP was exhibited for Ag/ZnO prepared by polyacrylamide gel method (A_nZ1) whose TEM and SEM images are shown in Figure 4. It is found that, the morphology of the A_nZ1 is different from A_nZ2 and A_nZ3. It is well known that the surface area of the A_nZ1 is also an important factor for its better photodegradation activity. The surface area of A_nZ1, A_nZ2 and A_nZ3 are 145, 87 and 23 $m^2 g^{-1}$ respectively. The A_nZ1 with hollow fluffy structure possesses the largest specific surface area, thus providing the largest number of active sites during the photocatalytic reaction; meanwhile, such hollow fluffy structure is favorable to mass transport and adsorption of 4-NP which occurs not only on the outside surface of the catalyst but also on the wall of the inside lattices. On the contrary, low surface area means less available active sites, limiting the adsorption activation of reactants on the catalyst.

The content of Ag in the composites has obvious influence on the photocatalytic activity. So, by using polyacrylamide gel method, the effect of silver content on the photodegradation process was also investigated (Figure 7). The photodegradation efficiency of 4-NP is about 92%, 100%, 86% and 67% for 0.1% Ag/ZnO, 0.5% Ag/ZnO, 1% Ag/ZnO and 2% Ag/ZnO, respectively, when the reaction was performed under UV-light for 3h.
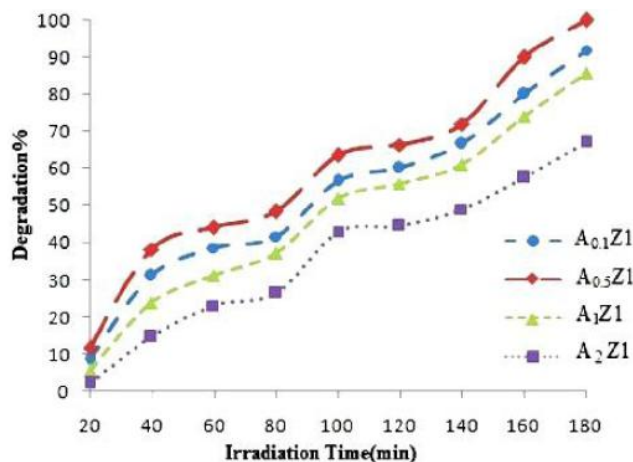

Figure 7 : Effect of silver content on the photocatalytic degradation of 4-NP prepared by polyacrylamide gel method.

The degradation percentage increases continuously as the silver content is increased up to a content level of 0.5% and then decreases with further increase of the content of Ag in the Ag/ZnO. Thus, the optimum Ag content is approximately 0.5%. The improved activity of Ag/ZnO is due to better charge separation of Ag/ZnO composites relative to pure ZnO. On the other hand, the incorporation of noble metal onto the ZnO surface increases the rate of electron transfer to dissolved oxygen. The photocatalytic activity of Ag/ZnO composites decreases when the content of silver reaches 1-2%. A possible reason is that silver particles also act as recombination centers at high silver deposition, which is caused by the electrostatic attraction of negatively charged silver and positively charged holes[44,45]. Thus, the presence of a proper content of silver can reduce electron–hole recombination and increase the photocatalytic activity. In addition, higher surface loadings of metal deposits may decrease the catalytic efficiency of the semiconductor due to the reductive availability of semiconductor surface for light absorption and pollutant adsorption[46], and the resultant variation of the surface hydroxyl content of Ag/ZnO with different Ag content. In the process of photocatalysis, after the photogenerated electrons and holes are separated from recombination, they can be trapped generally by the oxygen and surface hydroxyl, respectively, to produce ultimately the primary oxidizing species of the hydroxyl radicals (°OH), which plays a significant role in the photocatalytic oxidation process[47-49]. The more the surface hydroxyl content is, the more efficient the photocatalyst is[50]. From this point, we can reasonably con-

Full Paper

clude that the difference in photocatalytic activity is re-lated to various contents of surface hydroxyl on the hi-erarchically micro/nano-structured ZnO spheres caused by different Ag contents. Therefore, the 0.5% Ag/ZnO sample, which has the highest surface hydroxyl con-tent, exhibits the highest photocatalyst performance in our work.

TABLE 1 : The diameters of the E.Coli colonies on pure ZnO and AnZ1, AnZ2, AnZ3

Sample	D (mm)
	E. coli
Positive control	17.2±0.2
ZnO	12.5±0.2
A0.1Z1	0.5±0.1
A0.5Z1	0
A0.1Z2	2.0±0.2
A0.5Z2	1.5±0.2
A0.1Z3	6.5±0.2
A0.5Z3	4.5±0.2

Antibacterial activity

For demonstrating the antibacterial activity of as-prepared Ag/ZnO powders, E. coli was selected as the Gram-negative bacteria. TABLE 1 presents the diam-eters of the bacteria colonies on pure ZnO and Ag/ZnO nanostructures with different preparation meth-ods. Ag doped ZnO depicted the enhanced antibacte-rial property due to the photocatalysis and metal re-lease process[51–53]. When ZnO NPs (Eg = 3.39 eV) were under light irradiation, electron–hole pairs were generated. The hole (h^+) reacted with OH^- on the sur-face of NPs, generating hydroxyl radicals ($OH^•$), su-peroxide anion (O_2^-) and perhydroxyl radicals ($HO_2^•$). These highly active free radicals damaged the cells of microorganism as a result of decomposition and com-pletely destruction[54,55]. As shown in TABLE 1, under the condition of doping the same contents of Ag and ZnO, A_nZ1 presented much higher antimicrobial prop-erties than A_nZ2 and A_nZ3. The presence of transition metals Ag improved the charge transfer, reduced the chance of electron–hole pairs to recombine and pro-moted the generations of perhydroxyl radicals and other strong oxidizing materials[56,57]. Therefore, the presence of Ag enhanced antimicrobial ability of ZnO significantly. Among all the samples, the $A_{0.5}Z1$ sample showed ex-cellent antimicrobial activities. But considering the tox-icity of silver metal, the $A_{0.5}Z1$ sample was not perfect for the further applications. By contrast, the $A_{0.1}Z1$ sample also exhibited high antimicrobial activities indi-cating a better potential in medical and food packaging fields.

CONCLUSIONS

Ag/ZnO photocatalysts with different Ag loadings were prepared by photo reduction, chemical reduction and polyacrylamide-gel methods. The best photocata-lytic performance was exhibited for Ag/ZnO prepared by polyacrylamide gel method in comparison with chemical reduction and photo reduction method. It is because of the hollow fluffy structure and largest spe-cific surface area of this photocatalyst. An optimum Ag loading (0.5%) gave the fastest photodegradation of 4-NP and the reaction rate decreased at higher Ag load-ings. This is consistent with the presence of discrete Ag clusters leading to retarded recombination of the pho-toinduced electron–hole pairs. Decreasing activity at higher loadings is likely to arise from decreasing sur-face availability on the particles for reactant adsorption and light absorption.

ACKNOWLEDGEMENT

REFERENCES

[1] M.R.Hoffmann, S.T.Martin, W.Choi, D.W.Bahnemann; Chem.Rev., **95**, 69 (**1995**).

[2] R.Georgekutty, M.K.Seery, S.C.Pillai; J.Phys. Chem.C, **112**, 13563–13570 (**2008**).

[3] Y.H.Zheng, L.R.Zheng, Y.Y.Zhan, X.Y.Lin, Q.Zheng, K.M.Wei; Inorg.Chem., **46**, 6980–6986 (**2007**).

[4] Y.H.Zheng, C.Q.Chen, Y.Y.Zhan, X.Y.Lin, Q.Zheng, K.Wei, J.Zhu; J.Phys.Chem.C, **112**, 10773–10777 (**2008**).

[5] L.Jing, Z.Xu, X.Sun, J.Shang, W.Cai; Appl.Surf.Sci., **180**, 308 (**2001**).

[6] A.A.Khodja, T.Sehili, J.F.Pilichowski, P.Boule; J.Photochem.Photobiol.A: Photochem., **141**, 231-236 (**2001**).

Full Paper

[7] Y.Liu, C.Liu, Q.Rong, Z.Zhang; Appl.Surf.Sci., **220**, 7-11 **(2003)**.

[8] C.A.K.Gouveˆa, F.Wypych, S.G.Moraes, N.Dura´n, P.P.Zamora; Chemosphere, **40**, 427 **(2000)**.

[9] S.B.Zhang, S.H.Wei, A.Zunger; Phys.Rev.B, **63**, 075205 **(2001)**.

[10] H.J.Egelhaaf, D.Oelkrug; J.Cryst.Growth., **161**, 190 **(1996)**.

[11] A.Gulino, I.Fragala; Chem.Mater., **14**, 116 **(2002)**.

[12] K.K.Kim, H.S.Kim, D.K.Hwang, J.H.Lim, S.J.Park; Appl.Phys.Lett., **83**, 63 **(2003)**.

[13] K.Y.Gao, T.Seyller, L.Ley, F.Ciobanu, G.Pensl, A.Tadich, J.D.Riley, R.G.C.Leckey; Appl.Phys. Lett., **83**, 1830 **(2003)**.

[14] D.C.Look, G.M.Renlund, R.H.Burgener, J.R.Sizelove; Appl.Phys.Lett., **85**, 5269 **(2004)**.

[15] Y.J.Zeng, Z.Z.Ye, W.Z.Xu, D.Y.Li, J.G.Lu, L.P.Zhu, B.H.Zhao; Appl.Phys.Lett., **88**, 062107 **(2006)**.

[16] S.Limpijumnong, S.B.Zhang, S.H.Wei, C.H.Park; Phys.Rev.Lett., **92**, 155504 **(2004)**.

[17] X.Pan, Z.Ye, J.Li, X.Gu, Y.Zeng, H.He, L.Zhu, Y.Che; Appl.Surf.Sci., **253**, 5067 **(2007)**.

[18] F.X.Xiu, Z.Yang, L.J.Mandalapu, D.T.Zhao, J.L.Liu, W.P.Beyermann; Appl.Phys.Lett., **87**, 152101 **(2005)**.

[19] F.X.Xiu, Z.Yang, L.J.Mandalapu, D.T.Zhao, J.L.Liu; Appl.Phys.Lett., **87**, 252102 **(2005)**.

[20] R.Wang, J.H.Xin, Y.Yang, H.Liu, L.Xu, J.Hu; Appl.Surf.Sci., **227**, 312–317 **(2004)**.

[21] I.S.Kim, E.K.Jeong, D.Y.Kim, M.Kumar, S.Y.Choi; Appl.Surf.Sci., **255**, 4011 **(2009)**.

[22] Y.F.Yan, S.H.Wei; Phys.Status Solidi B, **245**, 641 **(2008)**.

[23] H.Xue, X.L.Xu, Y.Chen, G.H.Zhang, S.Y.Ma; Appl.Surf.Sci., **255**, 1806–1810 **(2008)**.

[24] V.Strikant, D.R.Clark; J.Mater.Res., **12**, 1425 **(1997)**.

[25] M.Sun, Q.F.Zhang, J.L.Wu; J.Phys.D: Appl.Phys., **20**, 3798 **(2007)**.

[26] B.D.Ahn, H.S.Kang, J.H.Kim, G.H.Kim, H.W.Chang, S.Y.Lee; J.Appl.Phys., **100**, 093701 **(2006)**.

[27] V.V.Shvalagin, A.L.Stroyuk, S.Y.Kuchimii; J.Nanoparticle Res., **9**, 427 **(2007)**.

[28] A.M.Galvan, C.T.Cruz, J.Lee, D.Bhattacharyya, J.Metson; J.Appl.Phys., **99**, 014306 **(2006)**.

[29] D.A.Neamen; Semiconductor physics and devices: basic principles, 3rd Edition, McGraw-Hill Professional, New York, **(2003)**.

[30] E.Hammarberg, A.Prodi-Schwab, C.Feldmann; J.Colloid Inter.Sci., **334**, 29 **(2009)**.

[31] S.F.Du, Y.J.Tian, H.D.Liu, J.Liu, Y.F.Chen; J.Am.Ceram.Soc., **89**, 2440 **(2006)**.

[32] S.Hartner, M.Ali, C.Schulz, M.Winterer, H.Wiggers; Nanotechnology, **20**, 445701 **(2009)**.

[33] X.M.Liu, G.Yang, S.Y.Fu; Mat.Sci.Eng.C, **27**, 750 **(2007)**.

[34] M.Khatamian, B.Divband, A.Jodaei; Materials Chemistry and Physics, **134**, 31-37 **(2012)**.

[35] M.Khatamian, A.A.Khandar, B.Divband, M.Haghighi, S.Ebrahimiasl; Molecular Catalysis A, **365**, 120-127 **(2012)**.

[36] Y.H.Zheng, L.R.Zheng, Y.Y.Zhan, X.Y.Lin, Q.Zheng, K.M.Wei; Inorg.Chem., **46**, 6980–6986 **(2007)**.

[37] W.W.Lu, G.S.Liu, S.Y.Gao, S.T.Xing, J.J.Wang; Nanotechnology, 19 **(2008)**.

[38] W.W.Lu, S.Y.Gao, J.J.Wang; J.Phys.Chem.C, **112**, 16792–16800 **(2008)**.

[39] J.Fan, R.Freer; J.Appl.Phys., **77**, 9 **(1995)**.

[40] R.Georgekutty, M.K.Seery, S.C.Pillai; J.Phys.Chem.C, **112**, 13563-13570 **(2008)**.

[41] A.L.Linsebigler, G.Q.Lu, J.T.Yates; Chem.Rev., **95**, 735–758 **(1995)**.

[42] X.Z.Li, F.B.Li; Environ.Sci.Technol., **35**, 2381–2387 **(2001)**.

[43] D.Li, H.Haneda; Chemosphere, **51**, 129 **(2003)**.

[44] V.Vamathevan, R.Amal, D.Beydoun, G.Low, S.McEvoy; J.Photochem.Photobiol.A, **148**, 233 **(2002)**.

[45] X.You, F.Chen, J.Zhang, M.Anpo; Catal.Lett., **102**, 247 **(2005)**.

[46] I.M.Arabatzis, T.Stergiopoulos, D.Andreeva, S.Kitova, S.G.Neophytides, P.Falaras; J.Catal., **220**, 127–135 **(2003)**.

[47] A.Mills, C.E.Holland, R.H.Davies, D.Worsley; J.Photochem.Photobiol.A, **83**, 257–263 **(1994)**.

[48] A.Sclafani, L.Palmisano, M.Schiavello; J.Phys. Chem., **94**, 829–832 **(1990)**.

[49] K.Chhor, J.F.Bocquet, C.Colbeau-Justin; Mater. Chem.Phys., **86**, 123–131 **(2004)**.

[50] W.Lu, S.Gao, J.Wang; J.Phys.Chem.C, **112**, 16792–16800 **(2008)**.

[51] Y.Inoue, Y.Kanzaki; The mechanism of antibacterial activity of silver-loaded zeolite, J.Inorg. Biochem., **67**, 377 **(1997)**.

[52] A.Bacchi, M.Carcelli, P.Pelagatti, C.Pelizzi, G.Pelizzi, F.Zani; Antimicrobial and mutagenic activity of some carbono- and thiocarbonohydrazone ligands and their copper(II), iron(II) and zinc(II)

complexes, J.Inorg.Biochem., **75**, 123–133 **(1999)**.

[53] Z.H.Yang, C.S.Xie, X.P.Xia, S.Z.Cai; Zn2+ release behavior and surface characteristics of Zn/LDPE nanocomposites and ZnO/LDPE nanocomposites in simulated uterine solution, J.Mater.Sci.Mater. Med., **19**, 3319–3326 **(2008)**.

[54] Y.Kikuchi, K.Sunada, T.Iyoda, K.Hashimoto, A.Fujishima; Photocatalytic bactericidal effect of TiO2 thin films: Dynamic view of the active oxygen species responsible for the effect, J.Photochem.Photobiol.A, **106**, 51–56 **(1997)**.

[55] B.Halliwell, J.M.C.Gutteridge; Oxygen toxicity, oxygen radicals, transition metals and disease, Biochem.J., **219**, 1–14 **(1984)**.

[56] A.Sclafani, M.Mozzanega, P.Pichat; Effect of silver deposits on the photocatalytic activity of titanium dioxide samples for the dehydrogenation or oxidation of 2-propanol, J.Photochem.Photobiol.A, **59**, 181–189 **(1991)**.

[57] G.Zhou, J.C.Deng; Preparation and photocatalytic performance of Ag/ZnO nanocomposites, Mater. Sci.Semicond.Process, **10**, 90–96 **(2007)**.